ICARUS **126,** 107–125 (1997)
ARTICLE NO. IS965630

UKIRT Observations of the Impact and Consequences of Comet Shoemaker–Levy 9 on Jupiter

BIANCA MARIA DINELLI[1]

Istituto di Spettroscopia Molecolare, CNR, Via Gobetti 101, 40129 Bologna, Italy
E-mail: bianca@ism1.ism.bo.cnr.it

STEVEN MILLER, NICHOLAS ACHILLEOS, HOANH AN LAM, MAURETTE CAHILL, AND JONATHAN TENNYSON

Department of Physics & Astronomy, University College London, Gower Street, London WC1E 6BT, United Kingdom

MARY-FRANCES JAGOD AND TAKESHI OKA

Department of Chemistry and Department of Astronomy and Astrophysics, University of Chicago, 5735 South Ellis Avenue, Chicago, Illinois 60637–1403

JEAN-CLAUDE HILICO

Laboratoire de Physique de l'Universite de Bourgogne, 6 Boulevard Gabriel, 21000 Dijon, France

AND

THOMAS R. GEBALLE

Joint Astronomy Centre, University Park, 660 N. A'ohoku Pl., Hilo, Hawaii 96720

Received May 22, 1996; revised August 30, 1996

The observation of Comet Shoemaker–Levy 9's collision with Jupiter in July of 1994 by the United Kingdom Infrared Telescope (UKIRT) produced spectroscopic data of high quality. Analysis of the data for Impact C has produced the first temperature curve that covers such an event, from the first visibility of the plume above the limb through to the settling down of the ejected gas onto the upper jovian atmosphere. Temperatures derived from methane emission show that 5 min after impact, a plume some 6500 km across was heated to ~1400 K. At its maximum spatial extent ~12 min after impact, a region of Jupiter's atmosphere ~45,000 km west from the impact site of the main Fragment C nucleus was heated sufficiently to show methane emission. Observations of impact sites from one jovian day onward showed that hot methane remained or was produced above the sites at least until July 27.

INTRODUCTION

The impact of Comet Shoemaker–Levy 9 (SL9) on Jupiter in July 1994 provided astronomers with a unique opportunity to observe the effects of a sizable cometary collision on a major planet. But uncertainties as to the exact sizes and densities of the impacting fragments (Weaver *et al.* 1995, Jewitt *et al.* 1993, Scotti and Melosh 1993) has made interpretation of the observations problematic. So in the absence of absolute impact energies, Hammel *et al.* (1995) devised a relative categorization making use of the observed effects. Their Class 1 impactors were Fragments G, K, and L. These produced large ejecta and impact plumes which reached a height of 3200 km above the ammonia ice cloud deck (taken as the zero point for height measurements). According to Lagage *et al.* (1995), the peak intensity from Fragment L was 13,000 Jy at 12 μm. Impact sites visible immediately after collision stretched more than 10,000 km across and they probably produced multiple-wave events (although usually only one passing wave was clearly visible). Class 2 included Fragments A, C, E, and H and produced plume heights of about 2900 km, with "medium" ejecta and 12-μm peak intensities between 1200 and 2500 Jy (Lagage *et al.* 1995). Impact sites varied between 4000 and 8000 km in diameter. Class 3 comprised Fragments B, D, Q2, and N and produced almost no visible plume or ejecta. Impact sites were all less than 3,000 km in diameter.

[1] Visiting Research Fellow, Department of Physics and Astronomy, University College London.

0019-1035/97 $25.00

According to Hammel *et al.* (1995), Class 2 Fragment C impacted on July 17, 1994, at 07:13:51 UT (±3 min). The impact was observed by a number of groups (Maillard *et al.* 1995, McGregor *et al.* 1996, Meadows *et al.* 1995, Orton *et al.* 1995, Takeuchi *et al.* 1995). Orton *et al* (1995) produced a lightcurve for the Fragment C impact from images of the event taken at 2.25 μm using the NASA Infrared Telescope Facility (IRTF), also sited on Mauna Kea. Direct comparison between our observations of Impact C and the IRTF data is clearly beneficial, since observing conditions were identical for both sets of observations. In addition, observations of Fragment C by Maillard *et al.* (1995) and Takeuchi *et al.* (1995) make useful comparisons, although these are less extensive than the IRTF imaging data.

The most striking feature of the IRTF lightcurve of Orton *et al.* (1995) is an intensity maximum some 10 min after impact. This maximum, generally known as ''the main event'' (see, e.g., McGregor *et al.* 1996), has been interpreted as being due to the plume reaching maximum visibility coupled with additional heating of the jovian upper atmosphere as the ejecta fell back onto it (Drossart *et al.* 1995). Prior to the Impact C main event, Takeuchi *et al.* (1995), observing at 2.35 μm, reported a single precursor at 07:13 [Orton *et al.* (1995) did not commence observations of Jupiter until 07:15]. For both sets of observers, the emission intensity began to rise steeply toward the main event at 07:17.

Takeuchi and co-workers' (1995) observations broke shortly after this because their detectors saturated. But at 07:22, Orton *et al.* (1995) reported a shoulder at 90% of the peak intensity. The lightcurve peaked at 07:23, before falling uniformly to below 5% of the peak intensity by 07:27. The light curves of both Orton *et al.* (1995) and Takeuchi *et al.* (1995) show a secondary peak (rising to just over 5% peak intensity) centered on 07:30. After 07:33, intensities for both sets of observers remained at 1–2% of peak intensity above the preimpact background as the impact site remained in view. The IRTF observations continued after 07:40 at a number of wavelengths; the site of Impact C was visible at all wavelengths longer than 2 μm until 09:00 when observing ceased. Maillard *et al.* (1995), using the Fourier transform spectrometer on the Canada–France–Hawaii Telescope, deduced that the plume temperature was between 750 and 1500 K 10 min after impact. Around 1 h after impact, McGregor *et al.* (1996) reported a ring around the Impact C site visible at wavelengths between 3 and 4 μm.

In addition to observations of Fragment C, there are several reports of other Class 2 impacts. Nicholson *et al.* (1995) produced a lightcurve for the R impact, showing two precursors, separated by about 60 sec, as well as the main event. Drossart *et al.* (1995) interpret these precursors as the meteor phase of the impacting fragment, heated to incandescence at the nanobar pressure level, followed by the fireball produced by the terminal explosion. Boslough *et al.* (1995) have also given a detailed interpretation of a typical lightcurve which matches the observations well. These features are consistent with models, such as that of Zahnle and Mac Low (1994).

The impact of the 21 fragments of Comet SL9 left scars on the surface of Jupiter that were visible at various wavelengths for a long time after the impacts themselves. According to West *et al.* (1995), impact site scars visible in the optical region of the spectrum 1 day after impact could be accounted for by absorbing aerosols spread from the level of 1 to 300 mbar. Also in the optical, Moreno *et al.* (1995) considered their impact site images to be due to aerosols at 350–450 mbar. In the ultraviolet, Clarke *et al.* (1995) reported that the absorbing aerosols were higher and more widely dispersed than their optical counterparts. In the infrared, Orton et al. (1995) showed that the aerosols were reflective between 3 and 4 μm, signifying that they were located reasonably high in the stratosphere, thus avoiding the absorption of solar infrared by jovian methane. They also reported the detection of enhanced ammonia over impact sites.

In this paper, we report on the impacts of Fragments B (probable nondetection) and C (detected) and on observations of the evolution of impact sites from one jovian day after impact onward, made using the United Kingdom Infrared Telescope (UKIRT) situated on Mauna Kea in Hawaii. To assess the impact of SL9 on the jovian ionosphere, we have made use in this paper of a new data set of global H_3^+ infrared emission data due to Lam (1995). This has enabled us to disentangle effects due to the comet itself from the generally variable behavior of Jupiter's ionospheric emission. To assist the reader, the longitudinal dependence of this emission for the south 40°, 45°, and 50° lines of latitude is plotted in Fig. 1.

We also present in this paper what we believe is the first full retrieval of a plume temperature curve for any of the impacts, that of Fragment C. We have been able to do this only because a new, high-temperature methane line list (Hilico *et al.* 1994) became available during the course of our data analysis. [Encrenaz *et al.* (1995) have reported a temperature curve for Fragment H, which commences some 15 min postimpact.]

UKIRT OBSERVATION PROCEDURE

All of the observations reported in this paper were made using the UKIRT facility near-infrared spectrometer, CGS4. This is a long-slit spectrometer that can be operated in both high-resolution echelle mode and moderate-resolution grating mode. The measurements for this paper were made in echelle mode with a resolving power $\lambda/\Delta\lambda \sim$ 15,000 (20 km/sec) and in grating mode with a resolving power $\lambda/\Delta\lambda \sim 1200$ (250 km/sec). At the time of the SL9

impacts, CGS4 was fitted with a 58 × 62-pixel InSb detector, which gave a spatial resolution of 2.12″ per pixel row along the direction of the slit in echelle mode. We combined this with a slitwidth of 1″, giving an equivalent spatial resolution on a plane perpendicular to the line of sight at the distance of Jupiter of ~7850 × 3700 km in echelle mode. The spatial resolution in grating mode was 1.54″ × 1.54″ equivalent to ~5700 × 5700 km. For the observations reported here, we aligned the slit east–west along the south 44° line of latitude, to cover the expected impacts and their subsequent scar sites, or along the central meridian from pole to pole.

All of our spectra were taken in the spectral window from 3.2 to 4.1 μm, with most of them covering the lower end of this wavelength range. This spectral range was chosen because it covers a number of important transitions of the fundamental ν_2 band of the H_3^+ molecular ion, first detected outside of the laboratory in the jovian auroras (Drossart *et al.* 1989) and since shown to be an important indicator of general ionospheric activity (Miller *et al.* 1994, Lam 1995). The background due to reflected solar infrared radiation in this wavelength region is normally extremely low, since absorption by the ν_3 and $\nu_2 + \nu_4$ bands of stratospheric CH_4 is almost total. Thus, the transitions of H_3^+ are clearly observable at all latitudes (Ballester *et al.* 1994). In addition to monitoring transitions of H_3^+, the aim of these observations was to attempt to detect transitions of metal-bearing radicals and molecular ions (e.g., OH, CH_3^+) that might have been produced by the pyrochemistry of the impacts.

Integration times were set at 10 sec per individual spectrum and the spectrum was sampled by physically translating the array in six steps of 1/3 pixels. This gave a spectrum of data points sampled at 1/3 resolution elements for a total observation of 60 sec. The lapse time for such a sampling was 90 sec, with overheads. Spectra were taken for Jupiter (object) and for the sky, offset 120′ from the planet to provide background subtraction. The complete spectra were combined into quads, object–sky–sky–object, and we carried out two quads per total observation. So individual spectra of the planet were taken either one after the other or with a time delay of about 3 min between the end of one and the commencement of another. To obtain a flux calibration and transmission standard, we observed BS5056, using integration times of 5 sec instead of 10 sec. These parameters were used for both the echelle and grating spectral observations.

Although normal procedure for dealing with UKIRT spectroscopic data is to analyze full observations—in our case consisting of two quads—it was clear that this would produce far too coarse a time scale for events for which intensities changed by orders of magnitude in the space of a minute. Therefore, for the observations of impacts B and C, we rereduced our data so as to analyze individual object–sky pairs.

Since our spectra all contained well-known H_3^+ lines, we used these to obtain wavelength calibrations of the individual rows, using the well-determined laboratory rest wavelengths (Kao *et al.* 1991). This enabled us to take into account the Doppler shifting due to Jupiter's centre of mass motion with respect to the Earth and the limb-to-limb variations due to the rotation of the planet.

Observations of the impacts had to be carried out during late afternoon, twilight, and early night, Jupiter setting below the UKIRT observation horizon at approximately 10:00 PM local time. Thus, observing conditions were sometimes far from ideal, particularly during late afternoon observations. [Note: Hawaii Standard Time (HST) is 10 hr behind UT. Local sunset was ~8:00 PM HST, 06:00 UT.]

To locate the S44° line of latitude, the telescope viewfinding camera was centered visually on the center of the planet. The telescope was then offset to center the slit along the impact latitude. This procedure was especially difficult during the late afternoon, when the visual seeing was poor and the contrast between Jupiter and the sky was rather low and it was accompanied by an error perpendicular to the slit of up to ±2″. But pointing accuracy improved as the sky darkened, so that this error was reduced to ±1″. Similarly, stellar images showed typical point-spread functions 2″ full width at half-maximum in the late afternoon, improving to 1″ after sunset. Unless specifically remarked on, the weather conditions for our observations were clear.

FRAGMENT B

Observation of the Fragment B impact was made using CGS4 in echelle mode. With the wavelength centered on 3.538 μm, we observed the behavior of the H_3^+ lines visible in our window [ν_2 $R(3,2^-)$ 3.5308 μm, $R(3,3^-)$ 3.5337 μm, $R(2,1^+)$ 3.5384 μm, $R(2,2^+)$ 3.5422 μm] and the background. The slit was aligned along the south 44° line of latitude, located as described above. Observations began on UT 1994 July 17 02:41, and ran through continuously until 04:27 (times in this and the following section are given in UT hh:mm or hh:mm:ss for July 17, 1994). During this observation period the central meridian longitude (c.m.l.) observed ranged from System III 315° through to 7° (λ_{III} = 315° through to 7°).

The fragment's arrival appeared to be marked by an increase in the intensity of the H_3^+ lines in the 3.538-μm window that we were monitoring, followed by a subsequent decrease in intensity after a further 10 min. Hammel *et al.* (1995) gave a timing for the impact of July 17 02:56 (±3 m). Our data showed that the H_3^+ emission in the detectors corresponding to the eastern limb (λ_{III} = 55°) was much higher than that corresponding to the western limb

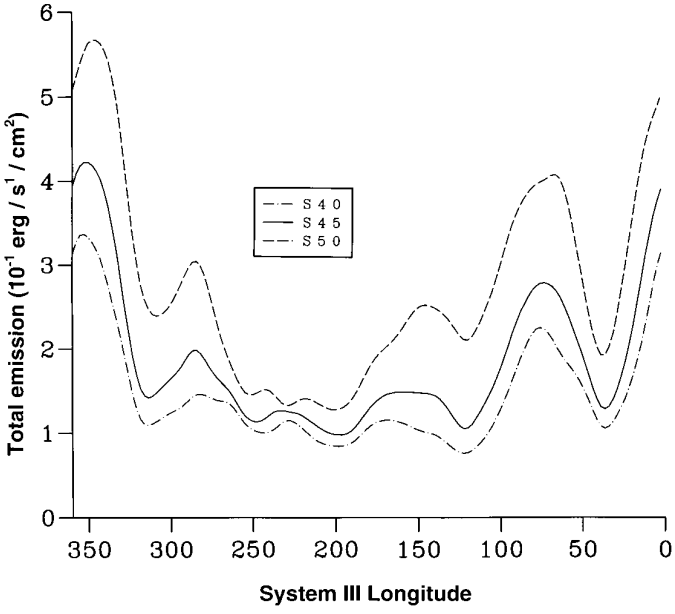

FIG. 1. Total H_3^+ emission around the south 45° line of latitude as a function of System III longitude, based on the 1993 data of Lam (1995).

($\lambda_{III} = 235°$) around impact time. The eastern intensity also appeared to peak at approximately 2:56 UT, apparently confirming the impact time deduced from the location of the impact site.

Unfortunately, the impact longitude of Fragment B ($\lambda_{III} = 71°$), (Hammel *et al.* 1995) coincided with a region where the southern auroral oval is at its most northernward extension, and the high magnetic dip angle is most conducive to the production of H_3^+ (Fig. 1). At the time of the collision, there were also difficulties in offsetting accurately to the impact latitude, because the observations had to be made prior to local sunset, and in maintaining accurate telescope tracking. A closer examination of our data showed that the chord subtended by the planet on our slit was decreasing as the time approached 2:56 UT indicating that the telescope tracking was drifting southward of the impact latitude.

It is clear from Fig. 1 that the effect of this would have been to produce a rise in the H_3^+ emission intensity. This effect would have been augmented by the inherent increase in intensity in the vicinity of $\lambda_{III} = 70°$, assuming that the general spatial variability of H_3^+ emission intensity was the same as in 1993. We therefore consider that the "normal" spatial variation of H_3^+ emission, coupled with the pointing difficulties already indicated, accounted for most of our intensity increase around impact time.

FRAGMENT C

UKIRT observations of the arrival and impact of Fragment C commenced at 06:20 UT on July 17, using CGS4 in echelle mode as for the Fragment B measurements. The improved seeing conditions that occurred after local sunset meant acquisition of the impact latitude was much more certain, a fact that was confirmed by the measurement of the planetary chord subtended on the slit. The data obtained comprise a continuous sequence through to 07:52, with the c.m.l. ranging from $\lambda_{III} = 89°$ through to 144°. This data set thus represents the most complete infrared spectral coverage of an impact at high resolution, giving important timing information on the various stages of the event. The importance of this is underlined by the fact that the Galileo satellite was not able to observe Impact C. A preliminary report of these data was made at the European SL9/Jupiter workshop, ESO, Garching, February 13–15, 1995 (Dinelli *et al.* 1995).

Spectral Analysis and Timing of Impact C

Figure 2 shows a sequence of spectral images taken before, during, and after the impact of Fragment C. The eastern limb of the planet was located in Row 23. Four lines due to H_3^+ were visible across the planet. Until 07:06:26 the spectra showed essentially a zero background across the entire planet and H_3^+ lines that were effectively constant (although there was spatial variation across the planetary disk). The figure shows that, after impact, the intensity of the spectra of the eastern side of the planet increased enormously, to the extent that the H_3^+ lines were very hard to discern, before the spectra returned to near their pre-impact levels. Before returning to this figure, however, we will look in more detail at the time evolution of the spectrum in Row 23.

The time series of spectra obtained from Row 23 is presented in Fig. 3. Spectrum 200, taken at 06:58:42, showed the typical intensities that prevailed on the eastern limb immediately prior to impact, both for the H_3^+ lines and for the continuum. But Spectrum 205, started at 07:06:26, showed an increase of ~70% in H_3^+ intensity in the row corresponding to the eastern limb ($\lambda_{III} = 207°$). This increase cannot be explained by the spatial variation of the H_3^+ emission at the impact latitude ($\lambda_{III} = 225°$); the Lam (1995) data set shows intensity decreasing as a function of increasing longitude toward $\lambda_{III} = 200°$, remaining approximately constant until increasing again around $\lambda_{III} = 250°$. Moreover, the spatial variation of two consecutive spectra is minimal on the time scale of our measurements. Since, if anything, the arrival of cometary material should have the effect of chemically removing H_3^+ (Cravens 1994), reducing its column density, we ascribe this increase in intensity as being due to heating of the ionospheric gas. In the spectrum taken at 07:11:03 (No. 208 in our series for July 17), there was a noticeable increase in the continuum, in addition to a further increase in the observed intensity of the strongest H_3^+ line of ~50%. H_3^+ line intensi-

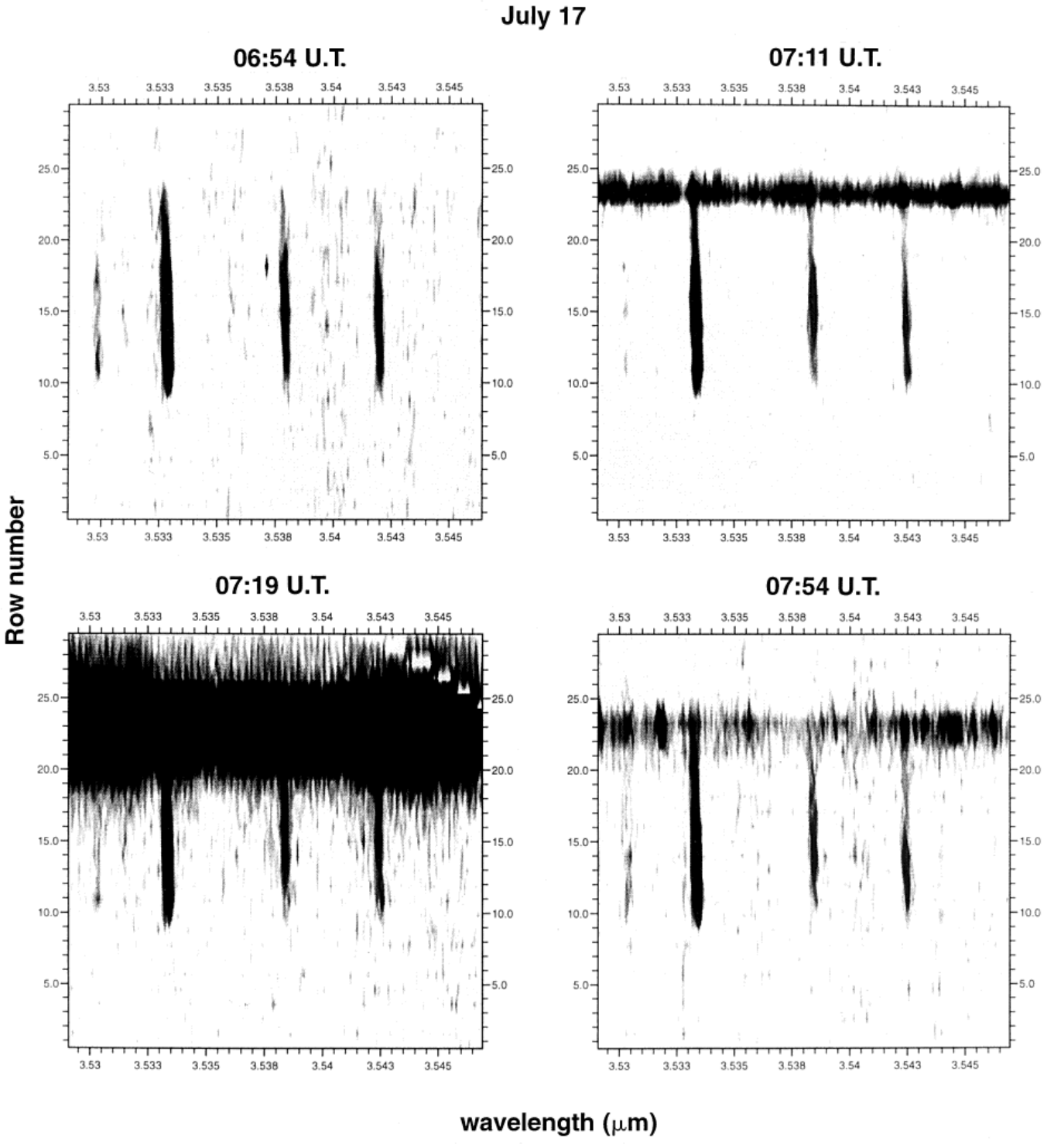

FIG. 2. UKIRT spectral images of Jupiter taken around the impact of Fragment C (July 17). The slit was aligned east–west along the south 44° line of latitude. The planet extends from the eastern limb in Row 23 to the western limb in Row 8. Wavelengths are in microns. (See text for further details.)

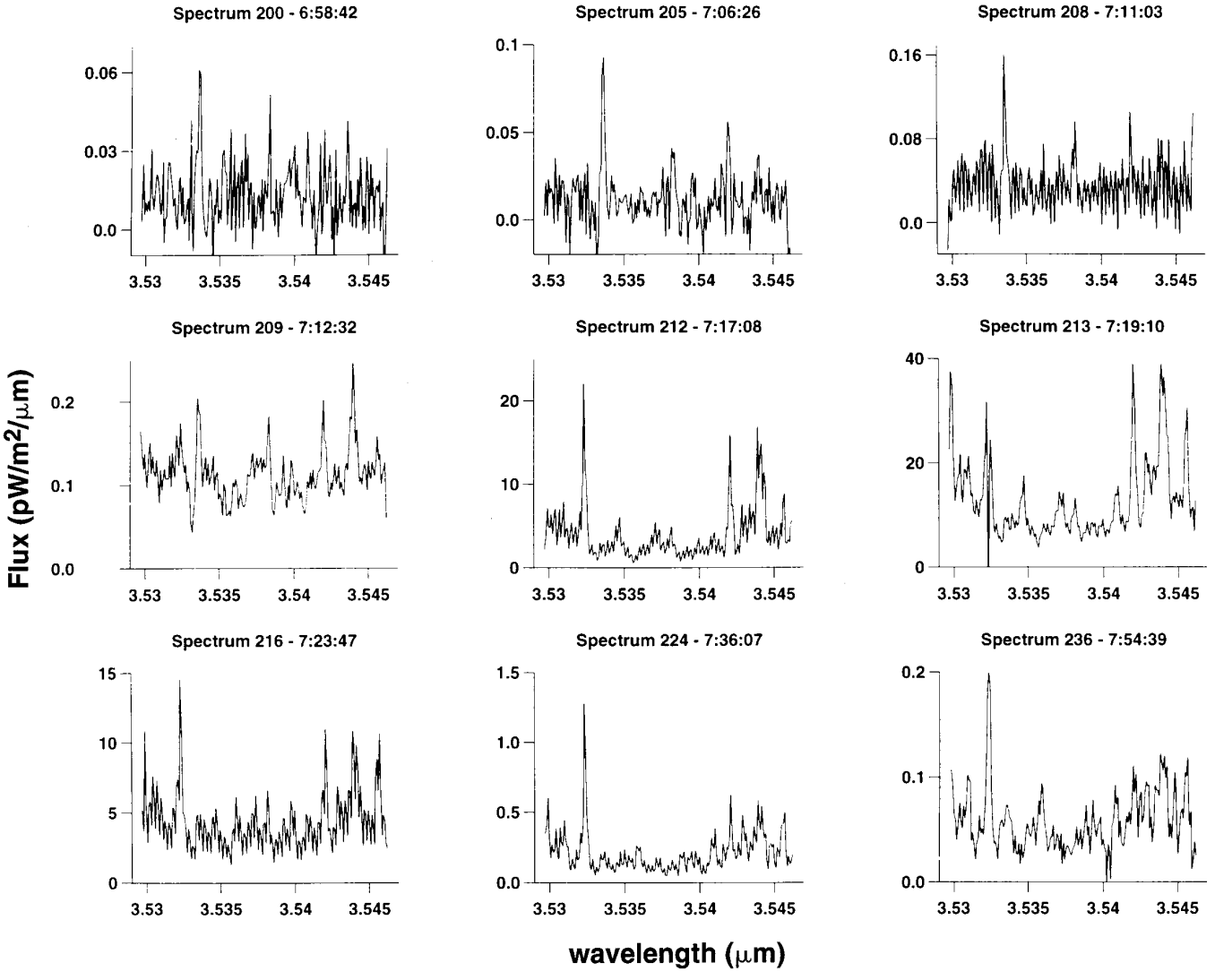

FIG. 3. Spectra of the eastern limb (Row 23) of Jupiter taken around the impact of Fragment C.

ties on the rest of the planet remained constant from Spectra 205 to 208.

While Spectrum 208 showed an increase in the continuum radiation, the next observation of the planet, Spectrum 209, starting at 07:12:32, had a very different appearance. Although the strongest of the H_3^+ lines, $R(3,3)$, was still visible at 3.534 μm, at longer wavelengths the spectrum was dominated by new features longward of 3.54 μm and there was additional structure throughout the whole wavelength range. We concluded that the spectrum was being produced by intense emission from high-J quintuplet structures of the P branch of the CH_4 ν_3 band. In particular, $P(18)$ accounted for the blue end of our spectrum and $P(19)$ for the red, transitions that had not been measured in the laboratory prior to SL9.

In Spectrum 209, there was also evidence of a $2\nu_2(0) \rightarrow \nu_2\, R(8,9^+)$ hot band transition of H_3^+ at 3.544 μm. Although this identification is complicated by the emerging methane $P(19)$ spectrum, we note two points:

1. If the intensity at 3.544 μm were due mostly to the H_3^+ hot band, its intensity relative to the ν_2 fundamental $R(3,3^-)$ (3.5337-μm) transition would signify a temperature of ~5000 K.
2. If it were due, on the other hand, to methane $P(19)$, the intensity of this feature relative to $P(18)$ would indicate either that the shorter wavelengths were being absorbed by a slightly cooler layer or that the gas was far from local thermal equilibrium.

Both identifications are somewhat problematic. At high temperature, the $2\nu_2(0) \rightarrow \nu_2\, R(8,9^+)$ hot band transition of H_3^+ should be accompanied by the $2\nu_2(2) \rightarrow \nu_2\, R(4,3^-)$

hot band transition, which would have shown up as a peak at 3.5385 μm, at least as intense as the neighbouring ν_2 fundamental $R(3,1^+)$ line. But this was not observed. On the other hand, attempts to model the conditions under which methane would provide the observed $P(19)/P(18)$ intensity ratio also proved unsatisfactory. Most probably, a combination of H_3^+ and CH_4 transitions were responsible for this line and its intensity in Spectrum 209 is evidence of very considerable heating in the upper atmosphere accompanying the impact, with temperatures reaching anywhere between 2000 and 5000 K.

Since the three spectra—205, 208, and 209—had very different characteristics, we attribute them to three distinct phases of the impact. The increased H_3^+ intensity seen in Spectrum 205, which was obtained during 07:06:26–07:07:54, accompanied by no increase in the continuum emission, was consistent with ionospheric heating prior to the explosion of the fragment itself. The increased continuum seen in Spectrum 208, however, is consistent with radiation from both the meteor phase and, more significantly, the terminal explosion of the fragment reflected from dust in the upper atmosphere (thus visible above the limb of the planet) as proposed by Drossart *et al.* (1995). (Note: the relative coarseness of our time sampling meant that we were almost certainly not able to separate these two events.) This would constrain our terminal explosion time to between 07:11:03 and 07:12:31, within the bounds set by Hammel *et al.* (1995), but toward the start of their range (07:13:51 (±)3 min).

Material to form the impact plumes has been shown (Hammel *et al.* 1995) to have been ejected at a vertical speed of ~12 km/sec, making it visible above the limb of the planet after ~60 sec. We interpret the developing methane spectrum detected in Spectrum 209 as being due to this gas heated and mixed into the plume from either the stratosphere or the troposphere. This spectrum was taken between 07:12:32 and 07:14:00. This would set 07:13:00 as the latest time the terminal explosion could have occurred to allow for the 60 sec needed for the plume to be visible from Earth and register in our spectrum.

The absence of methane emission in Spectrum 208 suggests that the plume was not visible in that spectrum, and that the terminal explosion could not therefore have occurred before 07:11:31. The combined effect of these two spectra is to narrow down our range of terminal explosion times to 07:12:00 (±35 sec), allowing for the range of plume ejection velocities (Hammel *et al.* 1995). This time is slightly ahead of the precursor peak time (07:13) given by Takeuchi *et al.* (1995), but we note that their precursor is ~60% of its maximum intensity at 07:12 and that the results are therefore not inconsistent. Our timing, combined with the data of Takeuchi *et al.,* makes Fragment C one of the best timed impacts.

With the preceding timing of the terminal explosion, the increase in Spectrum 205 would be too early by at least 3 min to correspond to heating due to the meteor phase of Fragment C itself, which is either covered or just missed by Spectrum 208. But ionospheric heating could also have occurred as a result of the passage of the dust preceding the nucleus. Traveling with the nucleus at 60 km/sec, this would have traversed the region of the ionosphere where H_3^+ is dominant in ~10 sec. The heating of the ionosphere shown in Spectrum 205 may be explained if appreciable quantities of dust preceded the nucleus by ~10,000 km.

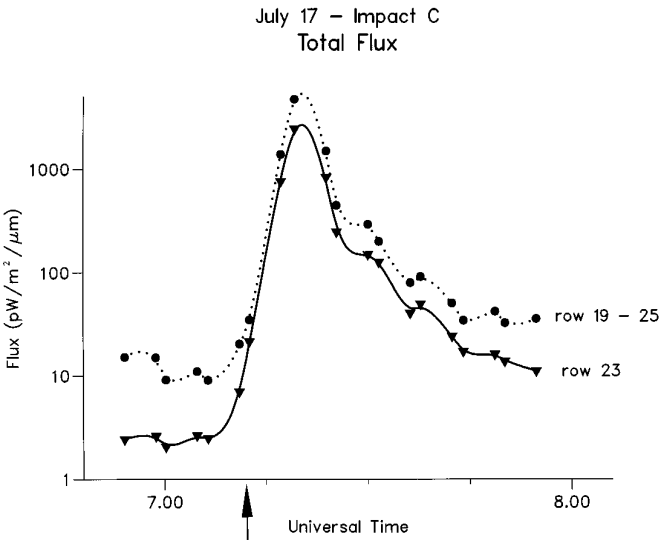

FIG. 4. Lightcurve for the Fragment C impact (July 17) derived from the spectral region covered by UKIRT derived from Row 23 and from the addition of Rows 19–25.

The lightcurve of Takeuchi *et al.* (1995), who continuously covered Impact C from ~12 min prior to impact until about 8 min after it, shows the main event (due to the rising plume) commencing at 07:17 UT, about 4 min after their precursor. The visibility of the methane spectrum in Spectrum 209 (timing 07:12:32–07:14:05) indicates that the rising plume started to be observable on UKIRT sometime ahead of observations using imaging techniques. We attribute this to the greater sensitivity of spectroscopy to weak emission above the background. After Spectrum 209, the H_3^+ lines were completely overshadowed on the limb of the planet by the strong methane spectrum, until $R(3,3)$ started to be visible once more in Spectrum 229 (07:43:56). During this time interval, the behavior of the methane spectrum enabled reliable temperatures to be derived.

Lightcurve

In Fig. 4, we present lightcurves derived by integrating the intensity across our spectral region for the brightest row, Row 23, and for all the affected rows, Rows 25–19. The time we derive for the impact is shown by the arrow.

Our time sampling was considerably coarser than that of Orton *et al.* (1995) and Takeuchi *et al.* (1995), and care must be taken in comparing the data. From the initial detection of the impact, the curve shows a rapid increase in intensity—more than two orders of magnitude in 9 min. Instead of the 90% shoulder observed by Orton *et al.* (1995) at 07:21, we find the maximum of our lightcurve. This reflects the difference in integration times between the UKIRT and IRTF observations, rather than any inconsistency between the two data sets.

Both the Row 23 and the total lightcurves show the shoulder around 07:30 detected by Orton *et al.* (1995) and Takeuchi *et al.* (1995). In addition, our data also indicate a second shoulder at 07:36 that is not apparent in the images. Drossart *et al.* (1995) proposed that shoulders in the lightcurves of various impacts could be explained by the first appearance of the impact site itself over the limb of planet. Computer graphics simulations of the evolution of the impact site as viewed from Earth show that (if the time of impact is as we estimate) the first shoulder corresponds to the first appearance of the impact site on the limb of the planet and the second to the complete appearance of the impact site on the limb. Alternatively, these shoulders could be due to the reentering plume ''bouncing'' on the upper jovian atmosphere (A. Fitzsimmons, private communication). At the end of our observations, some 40 min after impact, the spectra showed that the integrated intensity remained about three times the preimpact intensity throughout the spectral range as a result of the remaining continuum emission.

Temperature Retrieval

As stated above, increases in the H_3^+ emission intensity are most likely due to temperature effects rather than enhancement in the column density, since chemistry associated with the impacts would have tended to decrease H_3^+ concentrations (Cravens 1994). Analysis of the H_3^+ emission prior to and during the initial stages of impact shows that, if we assume an ambient ionospheric temperature of 800–900 K (Lam 1995), the temperature in the ionosphere increased by some 130–150 K as material ahead of the comet and the nucleus itself heated the ionosphere (Spectrum 205). The effect of the terminal explosion appears to have been to produce a further 190–280 K temperature increase (Spectrum 208). After that, it is difficult to separate the effects of the rising plume and the heated ionosphere, although it appears that temperatures averaged over our aperture were at least 2000 K in Spectrum 209. In what follows, we concentrate solely on temperature effects that can be ascribed to the plume, commencing with Spectrum 212 started at 07:17:08, about 5 min after our derived terminal explosion time.

Modeling the exact conditions within the expanding impact plumes is a considerable enterprise (Sekanina 1993, Zahnle and Mac Low 1994). Radiative transfer calculations showed that the emitting gas was high enough in the atmosphere that self-absorption was negligible. To derive effective temperatures as a function of time, therefore, it was assumed that local thermal equilibrium prevailed. We have also assumed that the gas distribution can be approximated by a pixel-averaged column density.

Although many rows of our detector were affected by the impact of Fragment C, it has so far only been possible to fit a temperature curve to the brightest spectra in Row 23. Our initial attempts to do this made use of the methane line list contained in the Hitran (Rothman *et al.* 1992) database. While this successfully identified the ν_3 $P(18)$ and $P(19)$ quintuplets, the intensities were poorly matched and an arbitrary and intense continuum was required. There were also several features that were simply not represented in the Hitran list (see Dinelli *et al.* 1995). During the course of the fitting, however, a new high-temperature line list due to Hilico *et al.* (1994) became available. This makes use of a new analysis of the CH_4 pentad system. Inclusion of these lines in the fit produced two important results:

1. A number of the unassigned lines were shown to belong to the $\nu_3 + \nu_4 \rightarrow \nu_4$ hot band.
2. The ''continuum'' was fitted by a ''grass'' of weak high-J, hot band, and overtone transitions that were not included in the Hitran list.

A comparison between the fitted spectrum and the observed data in Row 23 is shown in Fig. 5. In Fig. 5a, taken approximately 7 min after impact, as well as the $P(18)$ and $P(19)$ structures, the $P(17)$ and $P(18)$ $\nu_3 + \nu_4 \rightarrow \nu_4$ hot band lines were clearly discernible at 3.5346 and 3.5373 μm, respectively. [Note: Even with the Hilico *et al.* (1994) database, unassigned methane features remained in the SL9 data. These features have also been observed in high-temperature laboratory spectra of methane (P. Bernath, private communication).] But in Fig. 5b they were no longer present. Instead, part of the Q branch of the $\nu_2 + \nu_4$ combination band was visible. The exact behavior of these hot and overtone transitions is critical for the temperature retrieval process.

The fitting showed that the Hilico *et al.* (1994) line list accounted in general for much of what was observed. The fit was by no means perfect, however, and the relative intensity of some of the lines within the quintuplet was not well matched. This was a particular problem for the $P(19)$ lines. This problem cannot be explained by assuming a nonthermal distribution, since the relative intensities of members of an individual pentad structure are not temperature dependent. The spectrum could be modeled more accurately by assuming that the spectra were obtained looking tangentially at the plume through a layer of cooler ($T \sim 300$ K) gas, probably pushed ahead of the expanding

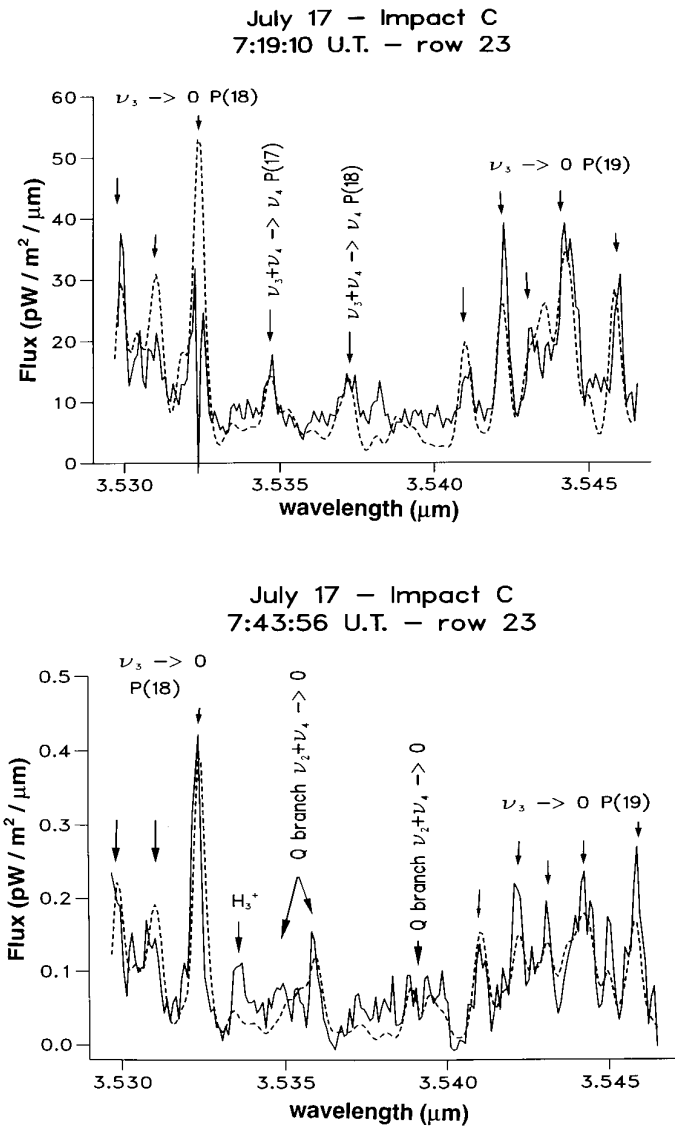

FIG. 5. Typical fitted spectra for Row 23 during the impact (July 17) of Fragment C, showing the spectral features most useful for the temperature fit.

plume (and possibly giving rise to large-scale effects; see later). Such modeling was computationally expensive, however and, once more, did not significantly affect the derived methane temperature.

To obtain a good temperature curve, we needed to fit this parameter (T) together with the average column density (ρ_{col}) in our pixel. With such a limited spectral range, however, T and ρ_{col} were highly correlated. The fundamental transitions $P(18)$ and $P(19)$ are not sufficiently sensitive to temperature differences once T is greater than ~600 K; however, at temperatures in excess of 1000 K, the hot band transitions become sufficiently intense for them to act as accurate temperature determinators. This is because the

TABLE I
Fitted Temperatures and Column Densities for the Limb Spectrum of Jupiter

Spectrum	Temperature (K)	Column Density (molecules cm^{-2})	Total Emission (erg sec^{-1} cm^{-2})
212	1406 ± 178	7.7 ± 1.0 × 10^{14}	77.96
213	1149 ± 82	37.7 ± 7.1 × 10^{14}	304.52
216	837 ± 80	36.8 × 10^{14}	127.73
217	699 ± 80	36.8 × 10^{14}	64.39
220	663 ± 80	36.8 × 10^{14}	51.67
221	647 ± 80	36.8 × 10^{14}	46.54
224	598 ± 20	23.0 ± 5.7 × 10^{14}	20.65
225	607 ± 12	24.9 ± 5.0 × 10^{14}	23.87
228	587 ± 11	16.5 ± 2.8 × 10^{14}	13.65
229	573 ± 14	14.5 ± 3.3 × 10^{14}	10.77
232	548 ± 10	19.5 ± 3.2 × 10^{14}	11.85
233	588 ± 11	9.6 ± 1.7 × 10^{14}	8.00
236	525 ± 10	19.5 ± 2.9 × 10^{14}	9.75

difference in the upper energy levels between the fundamental and hot band transitions is equivalent to ~4500 K. Below ~600 K, the hot band transitions no longer have any appreciable intensity, and their absence may be taken as an indication that temperatures are lower than this value. In the temperature regime 400–600 K, however, the $P(18)/P(19)$ intensity ratio becomes much more sensitive to the details of the temperature curve. The result of our fitting is shown in Table I, with the resulting temperature curve in Fig. 6. In Table I the total emission due to methane

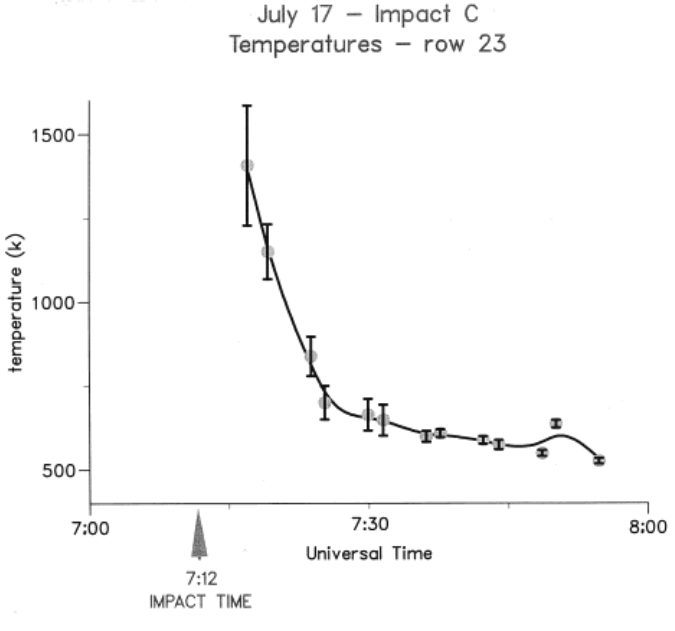

FIG. 6. Temperature curve for Fragment C impact (July 17) derived from the methane emission spectra of Row 23.

from the area covered by our detector has been computed from the Hilico *et al.* (1994) line list, assuming relative line emission intensities may be approximated by local thermal equilibrium.

The first spectrum in which the methane transitions were sufficiently intense for a good T/ρ_{col} fit to be obtained was Spectrum 212, taken at 07:17:08, 5 min after our derived impact time. For this we derived $T = 1406$ K (± 178 K). Two minutes later, at the point of maximum intensity, the temperature was 1149 K (± 82 K). These pixel-averaged temperatures are very reliable, since the intense hot band transitions in both spectra place stringent constraints on the fit. They are also in accord with the temperature derived from methane emission by Maillard *et al.* (1995). For the next two spectra, Nos. 216 and 217, the hot bands were still visible, but their intensity was difficult to ascertain accurately. To get temperatures for these, the pixel-averaged column density was fixed at just less than that derived for Spectrum 213. (This was also done for the next two, somewhat cooler spectra, Nos. 220 and 221.) After that, however, the hot bands were no longer visible and the $P(18)/P(19)$ ratio dominated the fit.

Figure 6 indicates that for the first 15 min after impact the temperature fell rapidly. This might be due to a phase of adiabatic plus radiative cooling of the expanding plume as suggested by Zahnle and Mac Low (1994). If we approximate

$$T(t) = T_0 \exp[-\alpha t]$$

for this initial phase of our temperature curve, we obtain values of $T_0 = 2250$ K (± 250 K) and $\alpha = 1.6$ (± 0.4) $\times$ 10^{-3} sec^{-1}. The temperature curve then shows that after 07:30, temperatures decreased by only $\sim$80 K over the next 25 min. This is probably indicative of collisional cooling with the surrounding atmosphere.

Spatial Effects

The sensitivity of CGS4 enabled effects from the impact to be detected across a greater extent of the planet than was visible in imaging data. In particular, in the brightest spectral image, No. 213, obtained about 8 min after impact, seven rows (25–19) contained spectra considerably different from the preimpact spectrum of the planet. These are shown in Fig. 7. Prior to impact, the intensity profile showed that the eastern limb of the planet was clearly located in Row 23 of our detector; this was also the case in spectra taken $\sim$40 min after impact. (This can also be seen from Fig. 2.) In what follows, therefore, we assume that the eastern limb was located in Row 23 throughout the impact. Row numbers decrease from east to west.

Row 25, whose center was located $\sim$16,000 km off the planet showed methane lines at about 2–3% of the peak intensity in Row 23 ($\lambda_{III} = 214°$); however, even after nightfall ($\sim$8 PM local time, 06:00 UT) there was some ''smearing'' of the planet due to seeing effects. The spectrum detected in Row 25, showing an intensity of $\sim$5% of Row 24, was probably consistent with this. The Row 24 spectrum, however, was some 60% of the intensity of Row 23. The timing of Spectrum 213 was consistent with (near) maximum plume height (Orton *et al.* 1995), and Row 24 thus contained emission from the plume rising above the limb of the planet.

Some of the intensity observed in Rows 22–19 (Row 18 showed an almost undisturbed, preimpact-type spectrum, dominated by H_3^+ lines) could be accounted for by the smearing of adjacent rows. Row 22 ($\lambda_{III} = 182°$), with an intensity of 5–10% of the Row 23 spectrum, probably also contained emission from the leading edge of the plume. But in Rows 21 ($\lambda_{III} = 168°$) to 19 ($\lambda_{III} = 147°$) it was noticeable that the red end of the methane spectrum [$P(19)$ dominated] became more intense than the blue end. The methane lines were also blue shifted by more than one resolution element, after correction for the line-of-sight velocity due to the planet's rotation, corresponding to velocities of 25($\pm$5) km/sec. In addition, a comparison of Row 26 (two rows from the bright Row 24) with Row 21 (two rows from the bright Row 23) shows the intensity in Row 21 to be almost an order of magnitude greater than that in Row 26. Taken together, these features strongly suggest that the spectra in Rows 21–19 were dominated by hot methane emission generated well inside the limb of the planet as viewed from Earth, and that smearing of the spectra of the more easterly rows was only a minor contribution to the observed emission.

A factor to be considered is that Row 22 also covered the location of Impact A ($\lambda_{III} = 188°$), which occurred the previous (jovian) day. Might Site A have become active at the point that the plume from Fragment C reached its zenith? We consider this highly unlikely. No emission from Site A was detected in the UKIRT spectra immediately prior to Impact C, when the site was already located inside the jovian disk, but before the spectral images became dominated by the impact.

Assuming the limb to be centered in Row 23, the center of Row 21 was located $\sim$45° in from the limb of the planet and, therefore, $\sim$55° from the original location of the impact site (which had rotated $\sim$5° in the 8 min after impact). These results therefore appear to indicate that a region of Jupiter's atmosphere at least 45,000 km from the impact site had been affected. If the plume material followed a ballistic trajectory with an initial velocity of 17 km/sec at 45° to the jovian vertical (Hammel *et al.* 1995), however, it could have travelled only 6000 km horizontally in 8 min.

According to Sekanina (1995), in January 1994 each fragment was associated with a tail which was at 30° to the direction of motion of the whole train; the tails of the

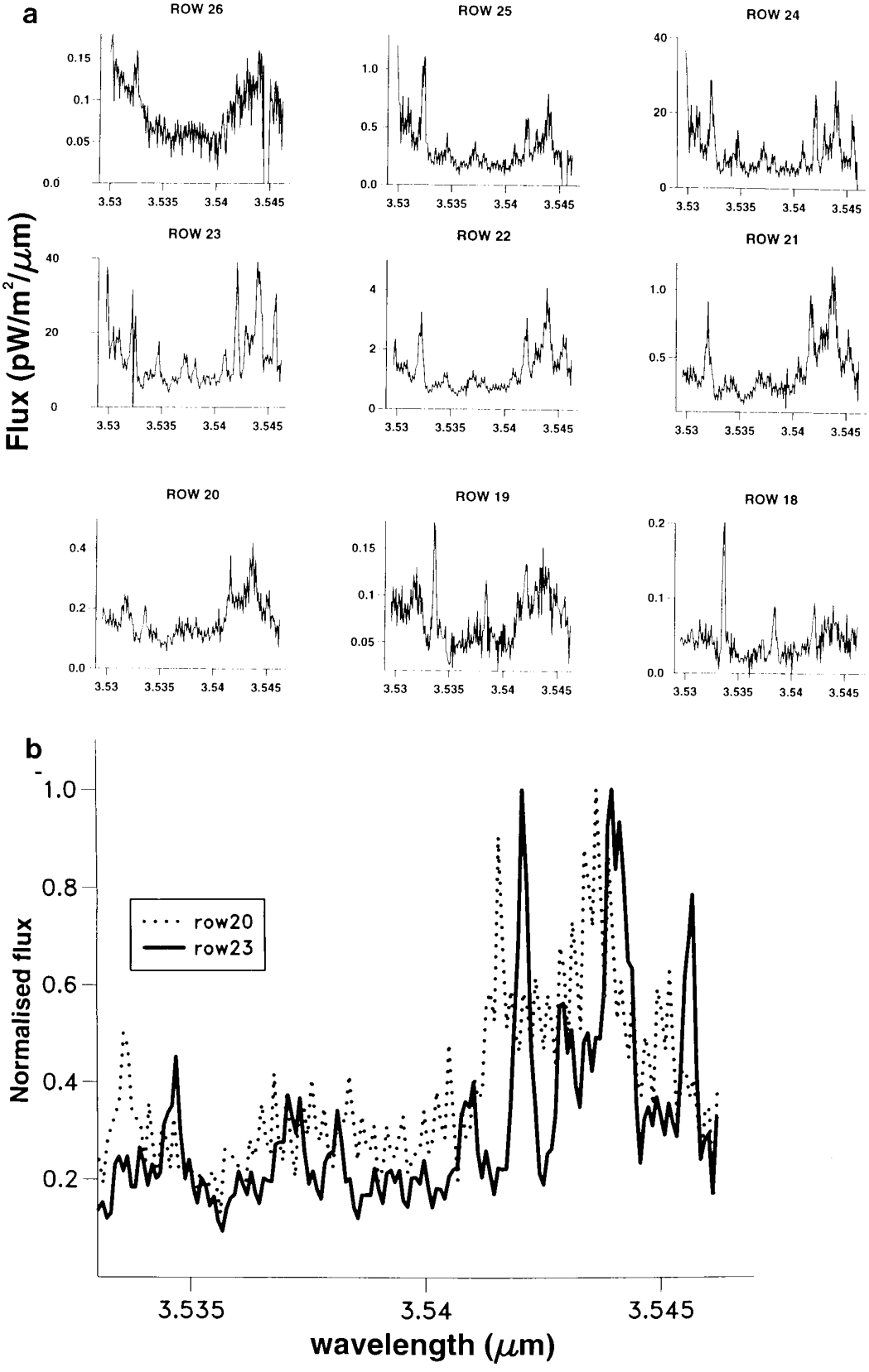

FIG. 7. Spectrum 213, July 17. (a) Jovian spectra obtained starting at 07:19:10 UT as a function of planetary location. The eastern limb was in Row 23 and lower row numbers correspond to more westerly locations. Comparison between the Row 24 and Row 21 spectra or the Row 23 and Row 20 spectra clearly indicates the extent of the blue shift of the methane lines at lower row numbers. The strong lines in Rows 19 and 18 are due to ionospheric H_3^+. (b) Enlargement of the region around $P(19)$ for Rows 23 and 20. The intensities have been normalized to highlight the blue shift.

larger fragments extended some 100,000 km. Dependent on the angle that they finally made to the impact trajectory, material from the tail could have hit the upper atmosphere coincident with the fragment impact and could have heated the gas for a considerable distance from the impact center, causing a series of "mini-plumes."

This could be an explanation for the extensive atmospheric heating observed by UKIRT outside of the immediate area of Impact C. Atmospheric methane ejected at an angle of 45° to the vertical would, at the location of Row 21, have been traveling directly along the line of sight to Earth. The blue shifting seen could be accounted for if an ejection velocity somewhat higher than that deduced by Hammel *et al.* (1995) was assumed. Unfortunately, to our knowledge at least, no one has been able to ascertain the exact geometry of the fragment tail impacts.

Another explanation is that material ejected from the jovian atmosphere ahead of the expanding fireball could be heated on reentry into the stratosphere. This has recently been put forward to explain metal emission lines observed by the Isaac Newton Telescope on La Palma (Fitzsimmons *et al.* 1996). Sodium emission (Na I) peaked at around 15 min after impact (for Fragment L), coinciding with the assumed plume splashback time. The peaks in Mg I, Ca I, and Fe I occurred another 5 min later, corresponding to grains following a meteoritic trajectory. But these authors were still describing effects within a few thousand kilometers of the impact location and at postimpact times later than the UKIRT spectra 213.

More likely, however, is that our observations detected shock-heated gas traveling at very high velocities and at very high altitudes ahead of the plumes visible in the HST images of Hammel *et al.* (1995). To travel 45,000 km in the time available after Impact C, the material must have had a velocity of nearly 100 km/sec, faster than the jovian escape velocity (60 km/sec). Impacts are known to be capable of excavating considerable quantities of planetary atmosphere, ejecting them out into space. It is therefore possible that the SL9 impacts had this effect. The problem of reconciling a scenario placing material onto an unbound orbit with the UKIRT observations, however, is that the line-of-sight velocity for such a process would have been nearer 90 km/sec than 20–30 km/sec observed. One would have to assume (1) a process of ejection followed by near-symmetric radial expansion at high altitude to account for a line-of-sight velocity of just 20–30 km/sec, and (2) that the gas had been ejected hot to account for the emission. Models taking these effects into account are currently being investigated (Mac Low, private communication).

IMPACT SITES

In addition to the impact data described above, UKIRT also observed several of the impact sites during and immediately after Impact Week. Once more, CGS4 was used in both echelle and grating modes, and spectra were obtained with the slit aligned along the S44° line of latitude and along the c.m.l. from pole to pole. A number of wavelength settings were chosen and the sites of Fragments B, C, D, E, G, Q1, Q2, and R were observed.

South 44° Spectra

Data obtained on July 19 with the slit aligned along the S44° line of latitude showed signs of the impact scars left by previous impacts. Three spectral images were obtained. The first spectrum, No. 73, was obtained at moderate resolution ($\lambda/\Delta\lambda \sim 1200$) and covered 3.35–3.60 μm. The System III c.m.l. was 313° ($\lambda_{III} = 313°$). In Fig. 8a, the spectral image is shown. In Fig. 8b, the intensity of the 3.534-μm H_3^+ line, the total intensity at this wavelength, and the continuum intensity are plotted as a function of pixel position, with the east limb occupying Row 22 and the west Row 5. At the c.m.l. of our spectral image, the impact sites of Fragments C ($\lambda_{III} = 225°$), G ($\lambda_{III} = 27°$), and D ($\lambda_{III} = 34°$) should have been visible close to the limbs of the planet; the spatial resolution (1.5″) along the slit prevented the separation of the latter two.

Figure 8 indicates that the continuum was considerably enhanced over the Fragment G/D site located in Row 22, but remained constant (and nearly zero) across the rest of the planet, showing a barely discernible increase at Site C, which should have been in Row 6. The bright continuum in Row 22 was probably dominated by the contribution of the jovian day-old Class 1 Impact G site, together with a contribution from the older Class 3 Fragment D site. The continuum was clearly due to debris from the impacts, visible in infrared images in this wavelength range (Orton *et al.* 1995). Conversely, the H_3^+ line intensity remained fairly constant across the planet, increasing slightly toward the west, with a slight enhancement at G/D and a ~50% increase at C.

The H_3^+ intensity increase over Site G/D was not greater than could be accounted for by limb brightening and spatial variation (Lam 1995); however, the longitude of Site C was close to an H_3^+ emission minimum in the data of Lam (1995), which occurs at $\lambda_{III} \sim 235°$. The same limb brightening effect over Site C should have been similar to that over Site G/D. Allowing for this, the H_3^+ emission enhancement over Site C was roughly double that expected. But later spectra that did not include the Impact C site also showed similar limb brightening. This makes interpreting Spectrum 73 as showing a genuine H_3^+ emission enhancement over the site dubious, although detection of H_3^+ enhancement was reported by Schultz *et al.* (1995).

Figure 9 shows the spectrum across our wavelength range of Row 22, containing Sites G and D. The high level of the continuum was apparent, increasing to longer

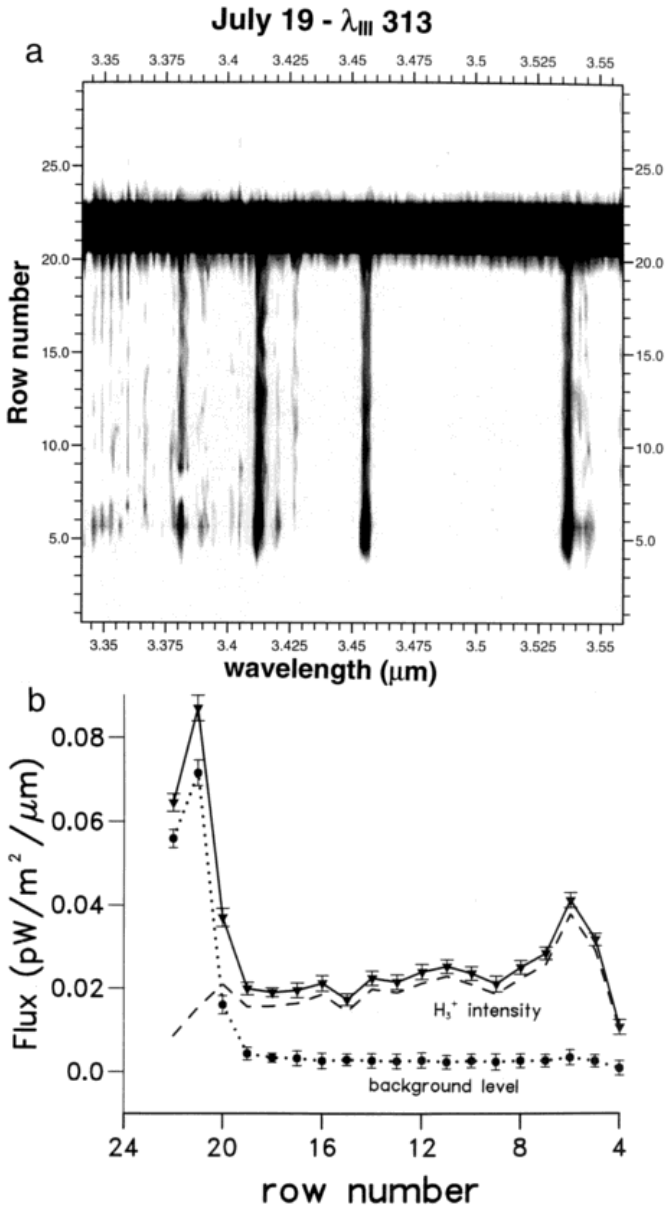

FIG. 8. (a) Spectral image obtained on July 19 at $\lambda_{III} = 313°$ with the slit aligned east–west along the impact latitude. The G/D Impact Site was clearly visible by the enhanced continuum in Row 22 (eastern limb). (b) Intensity profiles of the spectral image showing total intensity (solid line), H_3^+ intensity (dashed line), and continuum (dotted line). Central longitudes of the rows are: Row 23 $\lambda_{III} = 43°$, Row 22 $\lambda_{III} = 16°$, Row 21 $\lambda_{III} = 4°$, Row 20 $\lambda_{III} = 355°$, Row 19 $\lambda_{III} = 347°$, Row 18 $\lambda_{III} = 338°$, Row 17 $\lambda_{III} = 332°$, Row 16 $\lambda_{III} = 326°$, Row 15 $\lambda_{III} = 319°$, Row 14 $\lambda_{III} = 313°$, Row 13 $\lambda_{III} = 307°$, Row 12 $\lambda_{III} = 300°$, Row 11 $\lambda_{III} = 294°$, Row 10 $\lambda_{III} = 288°$, Row 9 $\lambda_{III} = 279°$, Row 8 $\lambda_{III} = 271°$, Row 7 $\lambda_{III} = 262°$, Row 6 $\lambda_{III} = 250°$, Row 5 $\lambda_{III} = 223°$.

wavelengths. But, in addition to the H_3^+ lines, absorption due to the methane ν_3 P branch was present, even after correcting for the effect of telluric absorption. This absorption was most pronounced at shorter wavelengths, around 3.4 μm (closer to the band center), where it was so strong that individual line absorptions were clearly visible. As a result of this absorption, the overall intensity of the continuum actually increased to longer wavelengths, rather than decreasing as would be expected from sunlight reflected by a layer of cometary debris. The longward extent of the spectrum indicated a temperature higher than that of the normal jovian stratosphere. The spectrum was best fitted using radiative transfer calculations by a layer of hot methane 260 km above the ammonia cloud deck, at a temperature of at least 300 K (although temperatures up 500 K also fit the data). The spectra also showed an additional deep absorption at 3.41 μm, which could not be accounted for by methane and was probably due to dust particles at the impact site.

The second July 19 spectrum, No. 91, was obtained at echelle resolution at the wavelength used for monitoring Impact C. The c.m.l. of the image was 334°, so Site C was no longer visible while G/D had moved further into the body of the planet. The spectral image and intensity profiles are shown in Fig. 10. Once more, these indicated that the continuum was significantly enhanced at the impact site. There was also a considerable limb brightening of the H_3^+ lines at the western limb. The spectrum at the impact site (Fig. 11) shows clearly the four H_3^+ fundamental lines seen normally in this window. Consistent with the moderate-resolution spectrum, at this wavelength there was no sign of methane absorption in the continuum, which fit a reflected solar spectrum.

The third spectrum at S44°, No. 117, was taken in echelle mode at a central wavelength of 3.254 μm at $\lambda_{III} = 4°$, as

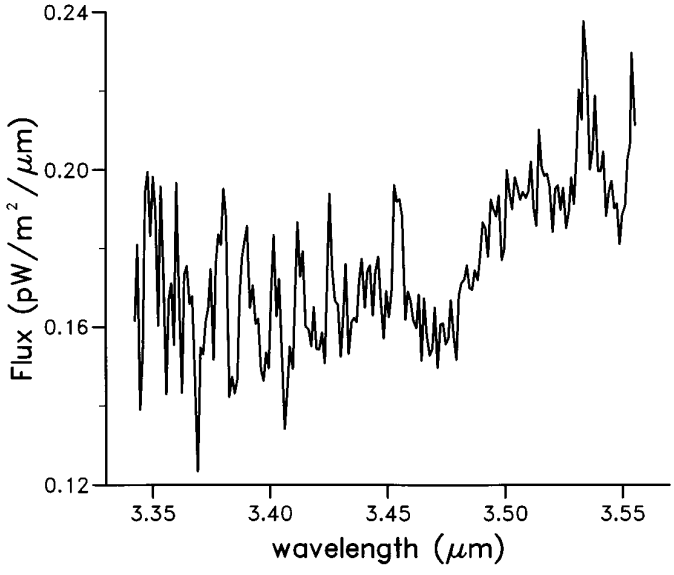

FIG. 9. Flux-calibrated spectrum of Row 22 $\lambda_{III} = 313°$ spectrum (Spectrum 73, Row 22, divided by fitted star spectrum) showing the deep absorption structure due to warm methane.

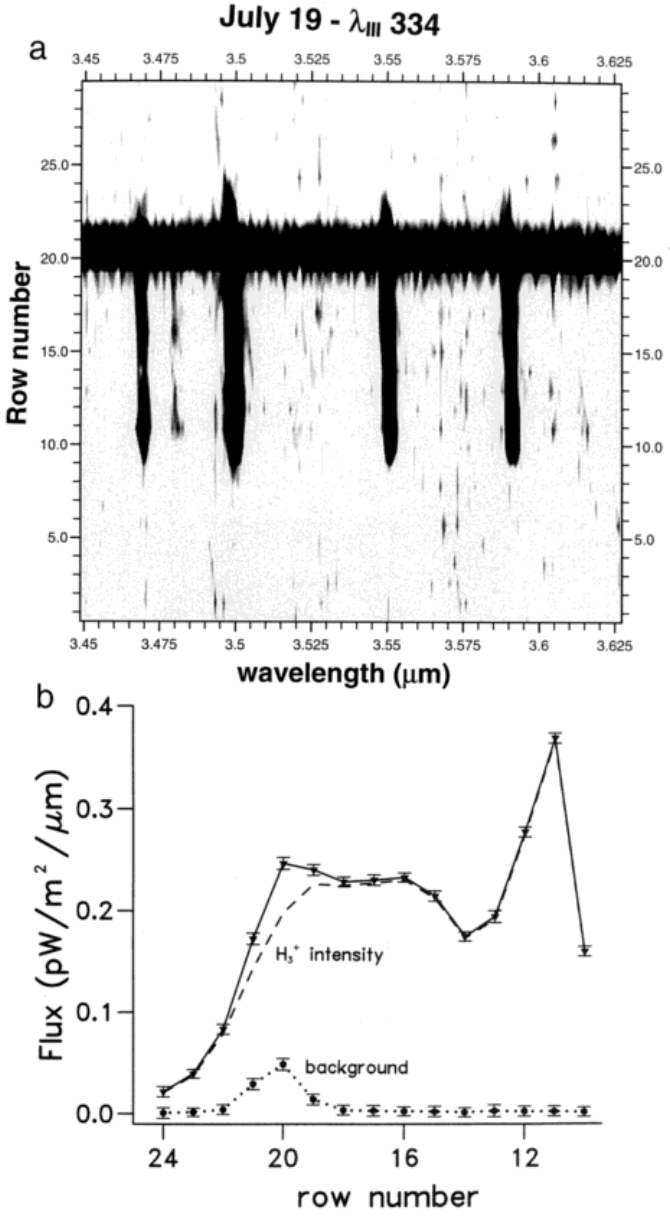

FIG. 10. As in Fig. 8, with $\lambda_{III} = 334°$. Site C was no longer visible and G/D had rotated onto the planetary disk. Central longitudes of the rows are Row 22 $\lambda_{III} = 64°$, Row 21 $\lambda_{III} = 35°$, Row 20 $\lambda_{III} = 20°$, Row 19 $\lambda_{III} = 9°$, Row 18 $\lambda_{III} = 359°$, Row 17 $\lambda_{III} = 351°$, Row 16 $\lambda_{III} = 342°$, Row 15 $\lambda_{III} = 334°$, Row 14 $\lambda_{III} = 326°$, Row 13 $\lambda_{III} = 317°$, Row 12 $\lambda_{III} = 309°$, Row 11 $\lambda_{III} = 299°$, Row 10 $\lambda_{III} = 288°$, Row 9 $\lambda_{III} = 273°$, Row 8 $\lambda_{III} = 244°$.

part of a search for CH-bearing molecular ions. The spectral image shown in Fig. 12 has one strong H_3^+ line at 3.257 μm and two weaker ones at shorter wavelengths, which do not match any known H_3^+ lines and may be due to incomplete absorption of the solar infrared. Close to the band center of CH_4 ν_3, this was a wavelength where a detailed spectrum of the methane absorption might have

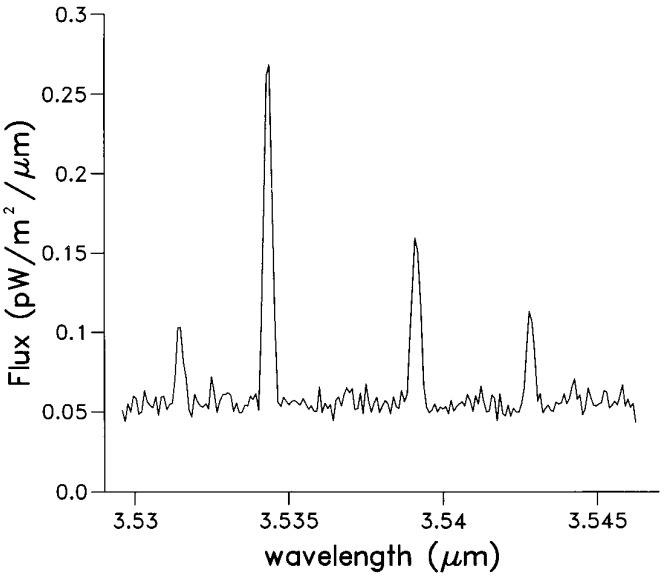

FIG. 11. Row 20 $\lambda_{III} = 334°$ spectrum (Spectrum 91) showing the enhanced continuum but no indication of methane absorption.

been obtained. Unfortunately only one stellar spectrum was obtained at this wavelength and it was not possible to remove atmospheric features to the accuracy required to apportion the absorption seen between telluric and jovian effects.

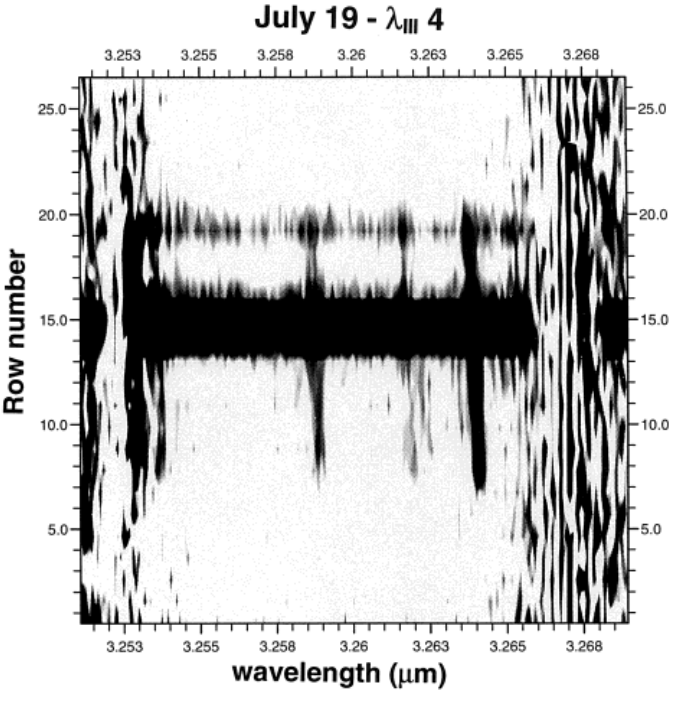

FIG. 12. East–west spectral image obtained on July 19 at $\lambda_{III} = 4°$. The G/D Impact Site was clearly visible by the enhanced intensity in Rows 19–16, indicating a spatial extent of ~30,000 km. The continuum was detectable over Site B on the eastern limb.

Figure 12 shows that the enhanced continuum over Site G/D extended across four rows, indicating an extent of some 8″ or 30,000 km. On the eastern limb was another region of enhanced continuum emission. We ascribe this to the site of Impact B, which Hammel *et al.* (1995) put at $\lambda_{III} = 70°$. As well as some increase on the western limb, there appeared to be H_3^+ emission enhancement over the G/D site in this spectrum; however, the longitudes of these impacts ($\lambda_{III} = 27°$ and $\lambda_{III} = 34°$, respectively) nearly coincide with a maximum in the Lam (1995) data set of H_3^+ emission and the increase may be explained by this.

Pole-to-Pole Spectra

On July 25 and July 27, spectra were obtained at a number of wavelengths in the 3- to 4-μm window, at both echelle and grating resolution, with the CGS4 slit aligned pole to pole along the central meridian. While the primary purpose of this was to monitor the behavior of the jovian auroras and to search for novel chemical species, the program enabled us to locate and study further the scars left after the week of impacts. A typical series of results are shown in Fig. 13, starting at 04:03 UT on July 25. At a c.m.l. of 129°, the impact site from Fragment E, put in Class 2 by Hammel *et al.* (1995) and located by them at $\lambda_{III} = 149°$, is just visible as a slight enhancement of the continuum in Row 6 above which the H_3^+ emission lines are superimposed.

At the impact latitude, 1.5″ (the width of the spectrometer slit) approximated to 6.5°. To be visible in this spectrum, the impact site must have extended at least 16° (at least 13,500 km) from the original impact site. Optical images of the site indicated it to be about 7° across on July 23 and more than 15° on July 30 (Hammel *et al.* 1995); in the ultraviolet, however, the scar already extended 13° on July 21, confirming Clarke and co-workers' (1995) statement that the absorbing aerosols were higher and more widely dispersed. The intensity of the continuum increased with the following two CGS4 spectral images, taken at c.m.l. of 135° and 143° respectively and then leveled off at c.m.l. 150°, before becoming almost invisible at c.m.l. 157°, the last spectral image in which it could be detected. This longitudinal asymmetry about the nominal impact longitude was typical of the westward drift of debris seen in images of the sites.

As well as the longitudinal properties of the impact sites, it is useful to look at the spectral variation as a function of latitude. In Fig. 14, the spectra of Row 6, corresponding to the impact latitude, and the two adjacent rows are shown for the spectral image obtained at c.m.l. 143°. The more southerly spectrum showed only emission due to H_3^+. But over the impact latitude the H_3^+ lines were superimposed on a continuum which, as in the case of the July 19 Site G/D spectrum, showed the effect of absorption by methane.

Once more, the longward extent of the CH_4 absorption features indicated that the gas was considerably hotter than the ambient $T \sim 180$ K normally associated with the region 1–300 mbar, in which West *et al.* (1995) located the aerosols and dust particles associated with the impact sites. This suggests two possibilities: (1) that the stratospheric methane remained ''hot'' for over a week after the fragment explosions; or (2) that the gas was being additionally heated by the solar infrared reflected back through it from the dust/aerosols. A combination of these effects could also have been possible. The spectra also showed the deep absorption at 3.41 μm.

The time evolution of the sites could also be probed using the data obtained from UKIRT. Spectra obtained at the impact latitude, and adjacent latitudes, at a c.m.l. of 50° are shown in Fig. 15. The data were obtained on July 25 and 27. At the longitude of the observations, the trailing edge of Site R ($\lambda_{III} = 39°$) and Q2 ($\lambda_{III} = 48°$) were possibly in view as was the leading edge of Site Q1 ($\lambda_{III} = 58°$). Unfortunately, the data of July 25 were somewhat spoiled by the effects of cirrus. Nonetheless, they did show a slightly enhanced continuum at the impact latitude as well as the H_3^+ lines, but no sign of methane absorption. On July 27, however, at the impact latitude there was a very visible continuum, once more showing strong methane absorption. This suggests that the warmer gas temperatures noted were being produced, at this stage, by reflected solar infrared, rather than by the residue of heating due to the impacts themselves.

CONCLUSIONS

Although a number of issues remain unresolved, this analysis of the SL9 data obtained at UKIRT has enabled us to add significantly to the description and interpretation of the events of July 1994. An important advantage of the UKIRT data set was the existence of high-resolution spectra taken throughout a Class 2 impact, enabling average plume temperatures to be retrieved from early on in the development of this feature. The sensitivity of the spectra to relatively low emission intensities allowed for subtle effects—temporal and spatial—to be registered. Knowledge of the planet's ''behavior'' at the wavelengths chosen, obtained from prior observation, assisted in separating the effects of the impacts and their aftermath from general jovian variability. In summarizing the UKIRT results, we look at two areas where they can make a particular contribution.

Class 2 Fragment Impact

If Fragment C was a ''typical'' representative of Hammel and co-workers' (1995) Class 2 impactor, the UKIRT data give the following scenario for these events. Setting $t = 0$ to be the time of the terminal explosion (note: due to our

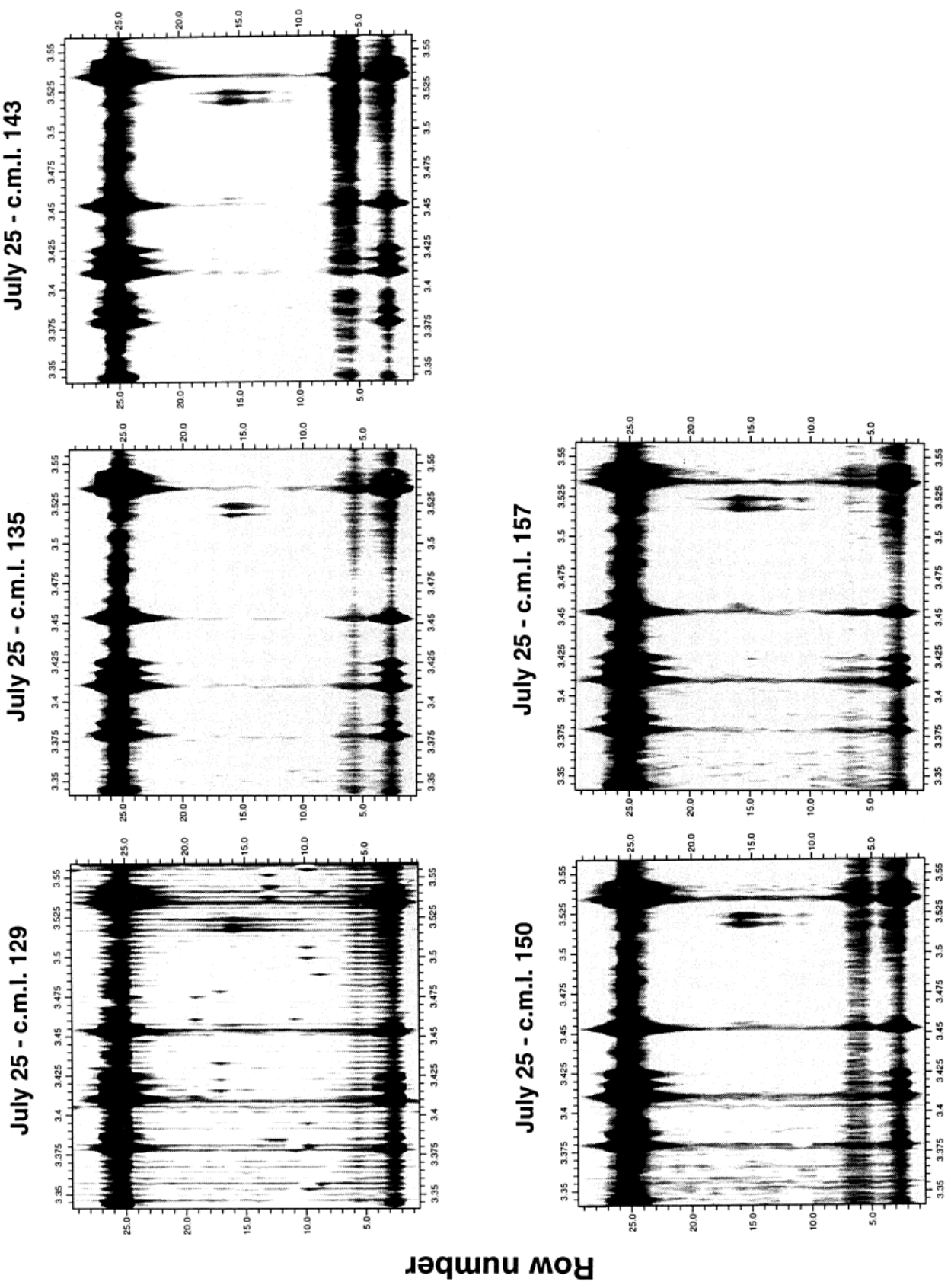

FIG. 13. Sequence of images taken with the slit aligned along the c.m.l. from north pole (Row 26) to south pole (Row 3) on July 25. Enhanced continuum emission from the impact site of Fragment E was visible from 04:03 UT until 04:50 UT in Row 6.

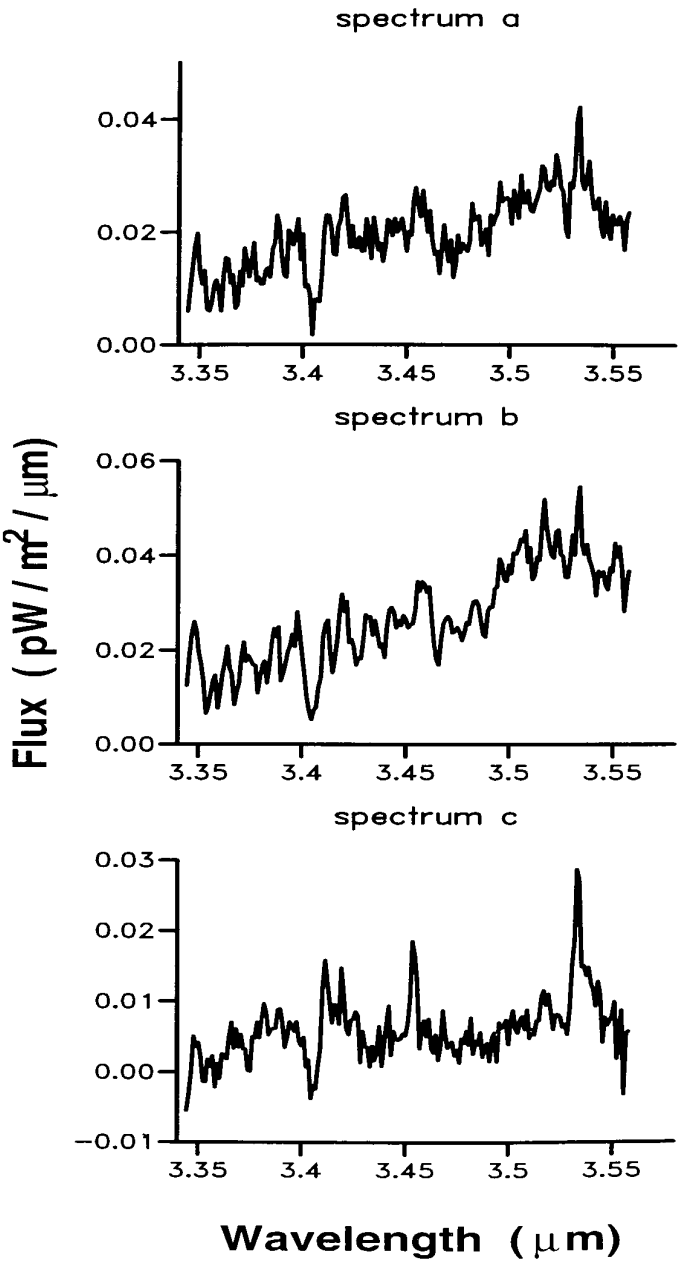

FIG. 14. Spectra obtained at $\lambda_{III} = 143°$ in (a) Row 7, 1.23″ north of Site E; (b) Row 6, over Site E; (c) Row 5, 1.23″ south of Site E. Evidence of warm methane absorption of the continuum was clear in all three spectra.

uncertainty in fixing the time of the terminal explosion, all the times given below are subject to an error of ±30 sec), we get the following:

1. $t = -330$ to -240 sec: The ionosphere was heated by 130–150 K as a result of cometary dust and small fragments passing through or impacting on it. This was the earliest effect of cometary arrival noted, and suggests that the coma extended for ~10,000 km ahead of the main fragment nucleus.

2. $t = -60$ to $+30$ sec: The ionosphere was heated by a further 190–280 K. Dust high enough in the atmosphere to be observed above the planetary limb reflected continuum radiation from the terminal explosion fireball.

3. $t = +30$ to $+90$ sec: The hot plume, rising at a minimum of 12 km/sec, appeared above the limb, entraining atmospheric methane. Additionally, it (shock?) heated the ambient ionospheric gas. Overall temperatures were between 2000 and 5000 K.

4. $t = 310$ to 400 sec: The plume extended some 6500 km across. The temperature of the extended plume material averaged ~1400 K and the gas was cooling adiabatically. This adiabatic cooling lasted until ~15 min after impact.

5. $t = 400$ to 490 sec. This period covered both the greatest intensity and the greatest spatial extent of the observed effects. At greatest extent, methane emission is observed from a region that, projected onto the planet's surface, is 45,000 km from the impact site. This effect may have been due to impact heating by tail material, precursor impactor, or expanding high velocity plume, but the exact cause is still unknown.

6. $t = 900$ sec onward: The impact region continued to cool slowly, T remaining in excess of 500 K for at least 40 min after impact.

Fragment Site Evolution

Again, if the UKIRT data were typical of the evolution of the various impact sites, the following behavior may be deduced:

1. $t = +0.1$–1.0 jovian day: The impact sites contained high level particles and/or aerosols overlaid with warm atmospheric gases, typically with temperatures in excess of 300 K and centered 260 km above the 600-mbar ammonia cloud deck. The report by Kim *et al.* (1996) that H_3 was depleted over fresh impact sites is consistent with this picture if "metal"-rich gas were high enough to be mixed into the ionosphere.

2. $t = +$ several jovian days: Over the impact sites themselves, warm gas was still to be found, again with temperatures in excess of 300 K. The appearance of absorption due to hot methane over regions of the atmosphere previously unaffected as infrared bright impact debris drifted (mainly) westward suggests that the gas was being additionally heated by the re-reflection of solar radiation.

3. As in the case of the particles causing absorption in the ultraviolet (Clarke *et al.* 1995), the infrared-reflecting particles also seem to have been higher than those producing the dark optical impact sites. They also spread out zonally at rates similar to the ultraviolet-absorbing debris. This conclusion is supported by comparison of meridional dispersion rates deduced from the ultraviolet images (Clarke *et al.* 1995) and the infrared auroral behavior (Miller *et al.* 1995).

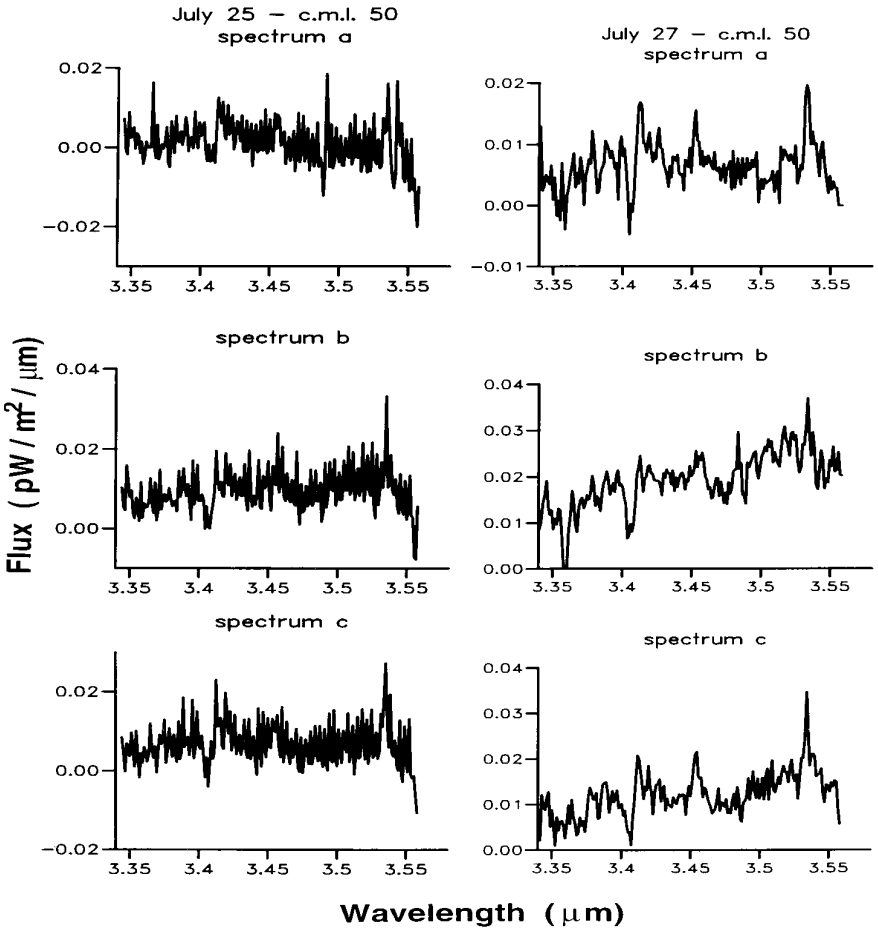

FIG. 15. Comparison of pole-to-pole spectra taken at $\lambda_{III} = 50°$ on July 25 and July 27: (a) Row 7, 1.23″ north of impact latitude; (b) Row 6, impact latitude; (c) Row 5, 1.23″ south of impact latitude. The effect of warm methane absorption was clearly visible on July 27 in Row 6.

ACKNOWLEDGMENTS

The authors would like to extend their thanks and congratulations to the staff of the United Kingdom Infrared Telescope in Hawaii, whose skill and dedication made this study possible. UKIRT is operated by the Royal Observatory Edinburgh on behalf of the U.K. Particle Physics and Astronomy Research Council (PPARC). Analysis of the July 1994 data was supported under PPARC Grant GR/K13684. B. M. Dinelli records her thanks to the Istituto di Spettroscopia Molecolare, CNR, for a leave of absence to work on these data at University College London. H. A. Lam was supported by a PPARC research studentship. M.-F. Jagod and T. Oka acknowledge support from the U.S. National Science Foundation under Grant PHY-93–21913. This paper has been significantly improved as a result of two anonomyous referees, whose assistance is gratefully acknowledged. We also thank Dr. Alan Fitzsimmons and Dr. Mordecai Mark Mac-Low for their helpful discussions.

REFERENCES

Ballester, G. E., S. Miller, J. Tennyson, L. M. Trafton, and T. R. Geballe 1994. Longitudinal variation of H_3^+ on Jupiter. *Icarus* **107,** 189–195.

Boslough, M. B., D. A. Crawford, T. G. Trucano, and A. C. Robinson 1995. Numerical modelling of Shoemaker–Levy 9 impacts as a framework for interpreting observations. *Geophys. Res. Lett.* **22,** 1821–1824.

Clarke, J. T., and 19 colleagues 1995. HST far-ultraviolet imaging of Jupiter during the impacts of Comet Shoemaker–Levy 9. *Science* **267,** 1302–1307.

Colas, F., D. Tiphene, J. Lecacheux, P. Drossart, B. de Batz, S. Pau, D. Rouan, and F. Sevre 1995. Near-Infrared imaging of SL9 impacts on Jupiter from Pic-du-Midi Observatory. *Geophys. Res. Lett.* **22,** 1765–1768.

Cravens, T. E. 1994. Comet SL9 impact with Jupiter: Aeronomical predictions. *Geophys. Res. Lett.* **21,** 11–14.

Dinelli, B. M., N. Achilleos, H. A. Lam, J. Tennyson, S. Miller, M.-F. Jagod, T. Oka, and T. R. Geballe 1995. Infrared spectroscopic studies of the impact of Fragment C of SL9. In *Proceedings of the European SL-9/Jupiter Workshop, Garching, February 13–15, 1995* (R. M. West and H. Boehnhardt, Eds.), pp. 245–249.

Drossart, P., and 11 colleagues 1989. Detection of H_3^+ on Jupiter. *Nature* **340,** 539–541.

Drossart, P., Th. Encrenaz, F. Colas, and P.-O. Lagage 1995. Interpretations of multiwavelength infrared observations of selected impacts: What did we see? In *Proceedings of the European SL-9/Jupiter*

Workshop, Garching, February 13–15, 1995 (R. M. West and H. Boehnhardt, Eds.), pp. 417–422.

ENCRENAZ, TH., R. SCHULTZ, J. A. STUWE, G. WIEDERMANN, P. DROSSART, AND J. CROVOISIER 1995. Near-i.r. spectroscopy of Jupiter at the time of Comet Shoemaker–Levy 9 impacts: Emissions of CH_4, H_3^+ and H_2. *Geophys. Res. Lett.* **22,** 1577–1580.

GRAHAM, J. R., I. DE PATER, J. G. JERNIGAN, M. C. LIU, AND M. E. BROWN 1995. The fragment R collision: W. M. Keck Telescope observations of SL9. *Science* **267,** 1320–1323.

FITZSIMMONS, A., P. J. ANDREWS, R. CATCHPOLE, J. E. LITTLE, N. WALTON, AND I. P. WILLIAMS 1996. Re-entry and ablation of cometary dust in the impact plumes of Shoemaker–Levy 9. *Nature* **379,** 801–803.

HAMMEL, H. B., AND 16 COLLEAGUES 1995. HST Imaging of atmospheric phenomena created by the impact of Comet Shoemaker–Levy 9. *Science* **267,** 1288–1296.

HILICO, J. C., J. P. CHAMPION, S. TOUMI, Vl. G. TYUTEREV, AND S. A. TASHKUN 1994. New analysis of the pentad system of methane and prediction of the (pentad–pentad) spectrum. *J. Mol. Spectrosc.* **168,** 455–476.

JEWITT, D., J. LUU, AND J. CHEN 1993. Physical properties of split comet Shoemaker–Levy 9. *Bull. Am. Astron. Soc*. **25,** 1042.

KAO, L., T. OKA, S. MILLER, AND J. TENNYSON 1991. A linelist for the astronomically important molecular ion H_3^+. *Astrophys. J. Supp*. **77,** 317–329.

KIM, S. J., G. S. ORTON, C. DUMAS, AND Y. H. KIM 1996. Infrared spectroscopy of Jupiter's atmosphere after the A and E impacts of Comet Shoemaker–Levy 9. *Icarus* **120,** 326–331.

LAGAGE, P. O., AND 15 COLLEAGUES 1995. Collision of Shoemaker–Levy 9 fragments A, E, H, L, Q1 with Jupiter: Mid-Infrared light curves. *Geophys. Res. Lett*. **22,** 1773–1776.

LAM, H. A. 1995. *Monitoring the Jovian Ionosphere Using H_3^+ as a Probe.* Ph.D. thesis, Univ. of London.

MAILLARD, J.-P., P. DROSSART B. BEZARD, C. DE BERGH, E. LELLOUCH, A. MARTEN, J. CALDWELL, J.-C. HILICO AND S. K. ATREYA 1995. Methane and carbon monoxide infrared emissions observed at the Canada–France–Hawaii Telescope during the collision of Comet Shoemaker–Levy 9 with Jupiter. *Geophys. Res. Lett*. **22,** 1573–1576.

MCGREGOR, P. J., P. D. NICHOLSON, AND M. G. ALLEN 1996. CASPIR observations of the collision of Comet Shoemaker–Levy 9 with Jupiter. *Icarus* **121,** 361–388.

MEADOWS, V., D. CRISP, G. ORTON, T. BROOKE, AND J. SPENCER 1995. AAT IRIS observations of the SL9 impacts and initial fireball evolution. In *Proceedings of the European SL-9/Jupiter Workshop, Garching, February 13–15, 1995* (R. M. West and H. Boehnhardt, Eds.), pp. 129–134.

MILLER, S., H. A. LAM, AND J. TENNYSON 1994. What astronomy has learned from H_3^+. *Can. J. Phys*. **72,** 760–771.

MILLER, S., AND 12 COLLEAGUES 1995. The effect of the impact of Comet Shoemaker–Levy 9 on Jupiter's aurorae. *Geophys. Res. Lett*. **22,** 1629–1632.

MORENO, F., AND 10 COLLEAGUES 1995. Physical properties of the aerosol debris generated by the impact of fragment H of P/Comet Shoemaker–Levy 9 on Jupiter. *Geophys. Res. Lett*. **22,** 1609–1612.

NICHOLSON, P. D., AND 12 COLLEAGUES 1995. Palomar observations of the R impact of Comet Shoemaker–Levy 9 on Jupiter. *Geophys. Res. Lett*. **22,** 1613–1616.

ORTON, G., AND 58 COLLEAGUES 1995. Collision of Comet Shoemaker–Levy 9 with Jupiter observed by the NASA Infrared Telescope Facility. *Science* **267,** 1277–1282.

ROTHMAN, L. S., AND 13 COLLEAGUES 1992. The Hitran database. *J. Quant. Spectrosc. Radiat. Transfer* **48,** 469–507.

SCHULTZ, R., TH. ENCRENAZ, J. STUWE, AND G. WIEDERMANN 1995. Monitoring of the near I.R. emission features at the NTT and detection of the northern counterparts. In *Proceedings of the European SL-9/ Jupiter Workshop, Garching, February 13–15, 1995* (R. M. West and H. Boehnhardt, Eds.), pp. 363–368.

SCOTTI, J. V., AND H. J. MELOSH 1993. Tidal breakup and dispersion of P/Shoemaker-Levy 9: Estimate of progenitor size. *Nature* **365,** 7333.

SEKANINA, Z. 1993. Disintegration phenomena expected during collision of Comet Shoemaker–Levy 9 with Jupiter. *Science* **262,** 382–387.

SEKANINA, Z. 1995. Nuclei of Comet SL-9 on images taken with HST. In *Proceedings of the European SL-9/Jupiter Workshop, Garching, February 13–15, 1995* (R. M. West and H. Boehnhardt, Eds.), 29–35.

TAKEUCHI, S., H. HASEGAWA, J. WATANABE, T, YAMASHITA, M. ABE, Y. HIROTA, E. NISHIHARA, S. OKUMURA, AND A. MORI 1995. Near-I.R. imaging of the cometary impact onto Jupiter. *Geophys. Res. Lett*. **22,** 1581–1584.

WEAVER, H. A., AND 20 COLLEAGUES 1995. The Hubble Space Telescope (HST) observing campaign on Comet Shoemaker–Levy 9. *Science* **267,** 1282–1287.

WEST, R. A., E. KARKOSCHKA, A. J. FRIEDSON, M. SEYMOUR, K. H. BAINES, AND H. B. HAMMEL 1995. Impact debris particles in Jupiter's stratosphere. *Science* **267,** 1296–1301.

ZAHNLE, K., AND M.-M. MAC LOW 1994. The collision of Jupiter and Comet Shoemaker–Levy 9. *Icarus* **108,** 1–17.